Supplement of The Cryosphere, 16, 3123–3148, 2022
https://doi.org/10.5194/tc-16-3123-2022-supplement

The Cryosphere Open Access EGU

Supplement of

Surge dynamics of Shisper Glacier revealed by time-series correlation of optical satellite images and their utility to substantiate a generalized sliding law

Flavien Beaud et al.

Correspondence to: Flavien Beaud (flavien.beaud@ubc.ca)

S1 Introduction

This supplement contains information supporting the reproducibility of the methods and some of the hypothesis made in the main manuscript. Section S2 (Methodology) contains details about the images used and their stacking in the data cube. Section S3 (Surge history of Mochowar and Shisper) details information about historical observations for both glaciers, estimation of lake volume, and surface velocity time series for Mochowar glacier. Section S4 (Discussion points) contains figures supporting some of the hypothesis made in the paper, including showing the effect of combining Landsat and Sentinel images, estimations of basal and surface melt, and the effect of choices of DEMs on the driving stress and its relationship with sliding.

The code for image correlation is available here http://www.tectonics.caltech.edu/slip_history/spot_coseis/download_software.html. The dataset and code used for the analysis and data plotting is available here https://doi.org/10.5281/zenodo.4624397.

S2 Methodology

S2.1 Image pairs and time span

Table S2.1 lists the details of all the image pairs used to make the velocity maps, as well as the time span between images. The subset of each image used can also be found in the data repository https://doi.org/10.5281/zenodo.4624397.

Table S2.1: Overview of image pairs used in this study. S2A and S2B stand for the Sentinel-2 A and B satellites, respectively, and LC stands for Landsat 8. The images are ordered by satellite system, then by date. The dates are in YYYY-MM-DD.

Pre-Ortho [date (platform)]	**Post-ortho** [date (platform)]	**Time span** [day]
2016-05-21 (S2A)	2016-07-20 (S2A)	60
2016-07-20 (S2A)	2016-10-28 (S2A)	100
2016-10-28 (S2A)	2017-04-16 (S2A)	170
2017-04-16 (S2A)	2017-05-06 (S2A)	20
2017-05-06 (S2A)	2017-07-25 (S2A)	80
2017-07-25 (S2A)	2017-11-02 (S2A)	100
2017-11-02 (S2A)	2017-11-07 (S2B)	5
2017-11-07 (S2B)	2017-12-07 (S2B)	30
2017-12-07 (S2B)	2018-01-01 (S2A)	25
2018-01-01 (S2A)	2018-01-21 (S2A)	20
2018-01-21 (S2A)	2018-02-05 (S2B)	15
2018-02-05 (S2B)	2018-03-07 (S2B)	30
2018-03-07 (S2B)	2018-03-17 (S2B)	10
2018-03-17 (S2B)	2018-03-22 (S2A)	5
2018-03-22 (S2A)	2018-04-01 (S2A)	10
2018-04-01 (S2A)	2018-04-06 (S2B)	5
2018-04-06 (S2B)	2018-05-01 (S2A)	25
2018-05-01 (S2A)	2018-05-11 (S2A)	10
2018-05-11 (S2A)	2018-05-21 (S2A)	10
2018-05-21 (S2A)	2018-05-26 (S2B)	5
2018-05-26 (S2B)	2018-06-05 (S2B)	10
2018-06-05 (S2B)	2018-07-10 (S2A)	35
2018-07-10 (S2A)	2018-07-15 (S2B)	5
2018-07-15 (S2B)	2018-07-25 (S2B)	10

Continued on next page

Table S2.1 – continued from previous page

Pre-Ortho	Post-ortho	Time span
2018-07-25 (S2B)	2018-08-04 (S2B)	10
2018-08-04 (S2B)	2018-08-14 (S2B)	10
2018-08-14 (S2B)	2018-08-24 (S2B)	10
2018-08-24 (S2B)	2018-08-29 (S2A)	5
2018-08-29 (S2A)	2018-09-08 (S2A)	10
2018-09-08 (S2A)	2018-09-13 (S2B)	5
2018-09-13 (S2B)	2018-09-18 (S2A)	5
2018-09-18 (S2A)	2018-09-23 (S2B)	5
2018-09-23 (S2B)	2018-10-23 (S2B)	30
2018-10-23 (S2B)	2018-10-28 (S2A)	5
2018-10-28 (S2A)	2018-11-07 (S2A)	10
2018-11-07 (S2A)	2018-11-17 (S2A)	10
2018-11-17 (S2A)	2018-12-02 (S2B)	15
2018-12-02 (S2B)	2018-12-07 (S2A)	5
2018-12-07 (S2A)	2019-03-07 (S2A)	90
2019-03-07 (S2A)	2019-04-01 (S2B)	25
2019-04-01 (S2B)	2019-04-06 (S2A)	5
2019-04-06 (S2A)	2019-04-21 (S2B)	15
2019-04-21 (S2B)	2019-05-01 (S2B)	10
2019-05-01 (S2B)	2019-07-20 (S2B)	80
2019-07-20 (S2B)	2019-07-25 (S2A)	5
2019-07-25 (S2A)	2019-07-30 (S2B)	5
2019-07-30 (S2B)	2019-08-04 (S2A)	5
2019-08-04 (S2A)	2019-08-09 (S2B)	5
2013-05-02 (LC)	2013-05-18 (LC)	16
2013-05-18 (LC)	2013-06-19 (LC)	32
2013-06-19 (LC)	2013-07-05 (LC)	16
2013-07-05 (LC)	2013-07-21 (LC)	16
2013-07-21 (LC)	2013-09-07 (LC)	48
2013-09-07 (LC)	2013-10-09 (LC)	32
2013-10-09 (LC)	2013-10-25 (LC)	16
2013-10-25 (LC)	2013-11-10 (LC)	16
2013-11-10 (LC)	2013-11-26 (LC)	16
2013-11-26 (LC)	2013-12-12 (LC)	16
2013-12-12 (LC)	2014-01-29 (LC)	48
2014-01-29 (LC)	2014-02-14 (LC)	16
2014-02-14 (LC)	2014-06-06 (LC)	112
2014-06-06 (LC)	2014-07-08 (LC)	32
2014-07-08 (LC)	2014-07-24 (LC)	16
2014-07-24 (LC)	2014-08-25 (LC)	32
2014-08-25 (LC)	2014-09-10 (LC)	16
2014-09-10 (LC)	2014-09-26 (LC)	16
2014-09-26 (LC)	2015-01-16 (LC)	112
2015-01-16 (LC)	2015-03-21 (LC)	64
2015-03-21 (LC)	2015-04-06 (LC)	16
2015-04-06 (LC)	2015-04-22 (LC)	16

Continued on next page

Table S2.1 – continued from previous page

Pre-Ortho	Post-ortho	Time span
2015-04-22 (LC)	2015-08-12 (LC)	112
2015-08-12 (LC)	2015-09-13 (LC)	32
2015-09-13 (LC)	2015-10-15 (LC)	32
2015-10-15 (LC)	2015-10-31 (LC)	16
2015-10-31 (LC)	2015-11-16 (LC)	16
2015-11-16 (LC)	2015-12-02 (LC)	16
2015-12-02 (LC)	2015-12-18 (LC)	16
2015-12-18 (LC)	2016-01-19 (LC)	32
2016-01-19 (LC)	2016-04-24 (LC)	96
2016-04-24 (LC)	2016-05-10 (LC)	16
2016-05-10 (LC)	2016-05-26 (LC)	16
2016-05-26 (LC)	2016-10-01 (LC)	128
2016-10-01 (LC)	2016-10-17 (LC)	16
2016-10-17 (LC)	2016-11-02 (LC)	16
2016-11-02 (LC)	2016-12-20 (LC)	48
2016-12-20 (LC)	2017-03-26 (LC)	96
2017-03-26 (LC)	2017-04-11 (LC)	16
2017-04-11 (LC)	2017-04-27 (LC)	16
2017-04-27 (LC)	2017-05-13 (LC)	16
2017-05-13 (LC)	2017-05-29 (LC)	16
2017-05-29 (LC)	2017-08-17 (LC)	80
2017-08-17 (LC)	2017-09-18 (LC)	32
2017-09-18 (LC)	2017-11-05 (LC)	48
2017-11-05 (LC)	2017-11-21 (LC)	16
2017-11-21 (LC)	2017-12-07 (LC)	16
2017-12-07 (LC)	2018-02-09 (LC)	64
2018-02-09 (LC)	2018-04-14 (LC)	64
2018-04-14 (LC)	2018-04-30 (LC)	16
2018-04-30 (LC)	2018-07-03 (LC)	64
2018-07-03 (LC)	2018-07-19 (LC)	16
2018-07-19 (LC)	2018-08-04 (LC)	16
2018-08-04 (LC)	2018-09-21 (LC)	48
2018-09-21 (LC)	2018-10-23 (LC)	32
2018-10-23 (LC)	2019-01-27 (LC)	96
2019-01-27 (LC)	2019-02-28 (LC)	32
2019-02-28 (LC)	2019-03-16 (LC)	16
2019-03-16 (LC)	2019-04-01 (LC)	16

S2.2 Velocity maps stacking

Figure S2.1 is a graphic representation of the stacking of image pairs on the data cube.

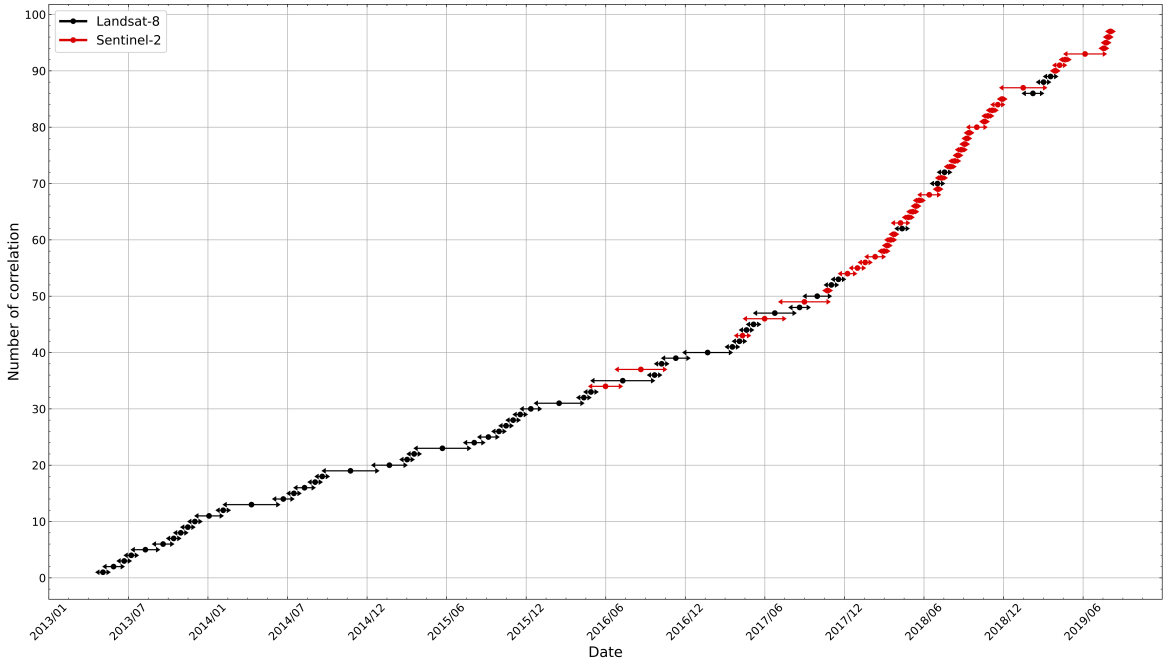

Figure S2.1. Time span distribution covered by image pairs denoted by arrows. Landsat 8 spans are in black and Sentinel-2 images are in red. All the correlations are sorted according to the youngest date, and then only the displacement maps, which cover the smallest period are selected. When staggering the velocity maps, each map is considered from the data of its older image until that of the date of the older image of the next velocity map.

S3 Results

S3.1 Surge history of Mochowar and Shisper

The Google Earth Engine timelapse video showing historical context for the two glaciers can be accessed at this link. The timelaspse shows that the two glaciers are still connected until 2006, after what the stagnant ice in front of Mochowar becomes apparent. In 2009, the two glaciers are clearly disconnected while a significant amount of stagnant ice is left in the valley. That ice completely disappears by 2014. In this timelapse, it is also apparent that Shisper surges from 1999 until 2005. While a significant terminus advance is apparent, it merely advances past the stagnant ice in the valley and stops $\sim 700\,\mathrm{m}$ up-valley from the most recent surge.

S3.2 Mochowar results

We present the surface velocity time series for Mochowar glacier (Fig. S3.1) as a reference to contextualize the surge of Shisper glacier. The image processing was done using the same parameters for both glaciers and was optimized for Shisper and the associated high velocities. The data for Mochowar is thus significantly more noisy, especially when snow cover is present. Spring speed-up events are present throughout the dataset, though (Fig. S3.1a). Surface velocities in the spring and summer

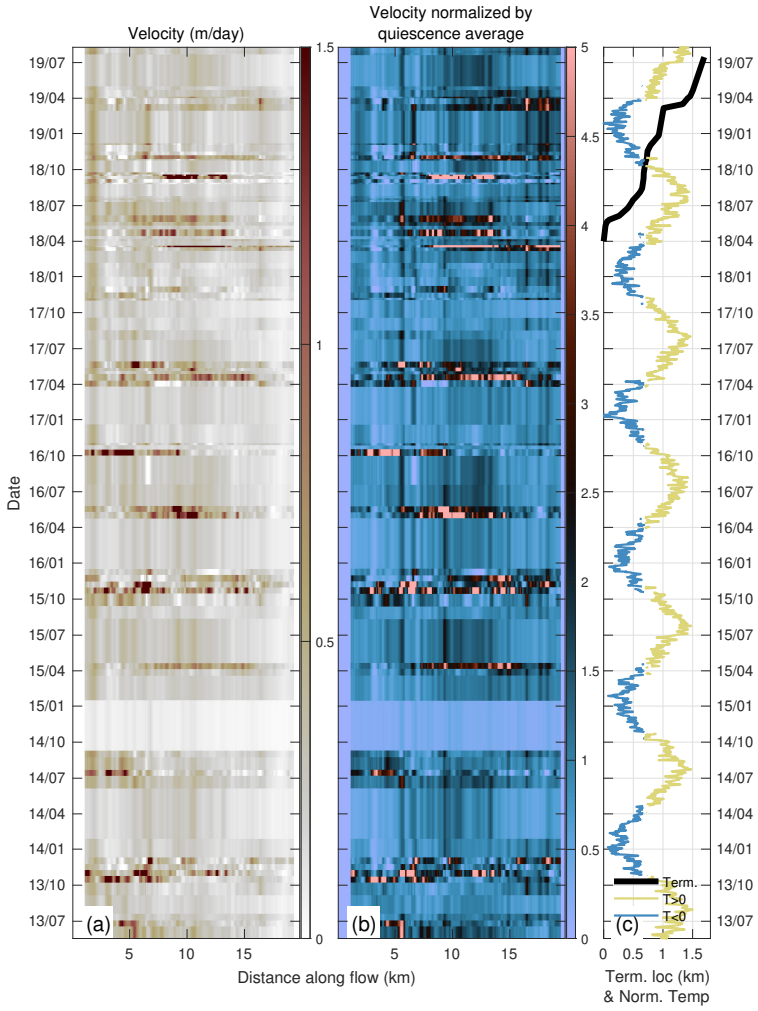

Figure S3.1. Time series of Mochowar glacier (a) surface velocities along the flowline (See Fig. 2 in manuscript) from 2013 to 2019 for Landsat 8 and Sentinel-2 imagery, (b) normalized surface velocities compared to pre-2018 velocity average, (c) MERRA-2 sat reanalysis temperature data and advance of Shisper terminus for reference.

consistently increase by a factor 2–5 (Fig. S3.1b). We cannot clearly identify a fall or winter speed-up for Mochowar, however, as the apparent velocity increase at that time is linked with snow cover or avalanches in the higher reaches. These dynamics are shown more simply in the spatially averaged velocities (Fig. S3.2).

S3.3 Determination of glacially dammed lake volume

A glacially dammed lake appears in November of 2018 (Shah et al., 2019) and drains on 28 June, 2019. We determine the lake's area by outlining lake in the RBG imagery from S2. We then evaluated the topography over the lake area to determine the lake's volume.

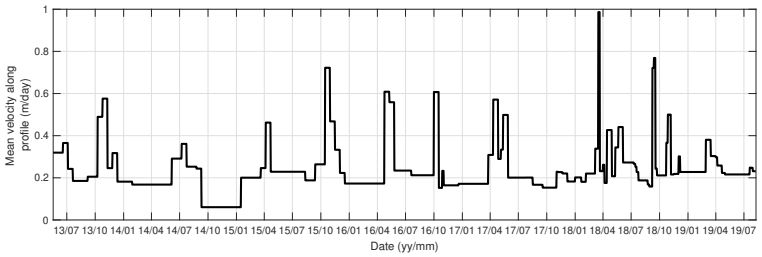

Figure S3.2. Spatial average of surface velocities along the profile of Mochowar glacier as a function of time. Note that the speed-up in fall / winter may be related to snow fall and not ice flow.

Table S4.1. Parameters used to calculate the shear heating based on estimates that would bracket the data presented in the main manuscript.

Relationship	u_t	σ_max	p	q
Main glacier low bound	$3\,\mathrm{m\,day^{-1}}$	$80\,\mathrm{kPa}$	2	1
Main glacier high bound	$0.4\,\mathrm{m\,day^{-1}}$	$500\,\mathrm{kPa}$	5	3

S4 Discussion points

S4.1 Combining Landat 8 and Sentinel 2 datasets

In the manuscript we only display the velocity timeseries from the composite of L8 and S2. To clearly highlight their respective importance, we show the two timeseries independently in Fig. S4.1.

S4.2 Estimations of surface and basal melt

In order to assess the relative contribution of basal and surface melt to initiate sliding changes we estimate melt rates from both basal shear heating and surface air temperature. The shear heating is calculated as proposed in Benn et al. (2019) and the surface melt based on a positive degree day factor. We use the basal shear stress calculated from the generalized sliding relationship and the parameter sets from Table S4.1. It is important to note that the shear heating is relatively steady in nature and mainly a function of sliding velocities. In contrast, the surface melt is highly seasonal.

S4.3 Effect of DEM and bed map on driving stress

The uncertainty surrounding the bed topography and ice surface elevation are one of the main source of uncertainty for estimating driving stresses. In order to asses the effect of ice geometry on the presented results, we plot Fig. 8 from the main manuscript using the SRTM DEM only (Fig. S4.4), the 2019 Worldview DEM only (Fig. S4.5), and the different bed elevations models (Fig. S4.3) available from Farinotti et al. (2019). While there are differences between the figures, they remain small and show qualitatively that the conclusion about the sliding relationship proposed in the manuscript hold regardless of DEM or bed map used. The figures and are summarized in Table S4.2.

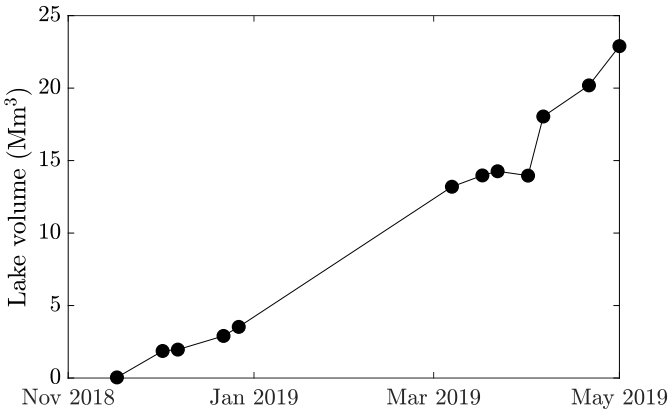

Figure S3.3. Estimated lake volume determined from lake areas and DEM.

Table S4.2. Overview of DEM and bed data combination used for plotting.

Figure	DEM	Bed data	Plot axis
Fig. S4.4	SRTM	Composite bed	x-lin; y-log
Fig. S4.5	2019 Worldview DEM	Composite bed	x-lin; y-log
Fig. S4.6	Combined DEMs	Bed model 1	x-lin; y-log
Fig. S4.7	Combined DEMs	Bed model 2	x-lin; y-log
Fig. S4.8	Combined DEMs	Bed model 3	x-lin; y-log
Fig. S4.9	Combined DEMs	Composite bed model	x-log; y-log
Fig. S4.10	Combined DEMs	Composite bed model	x-lin; y-lin

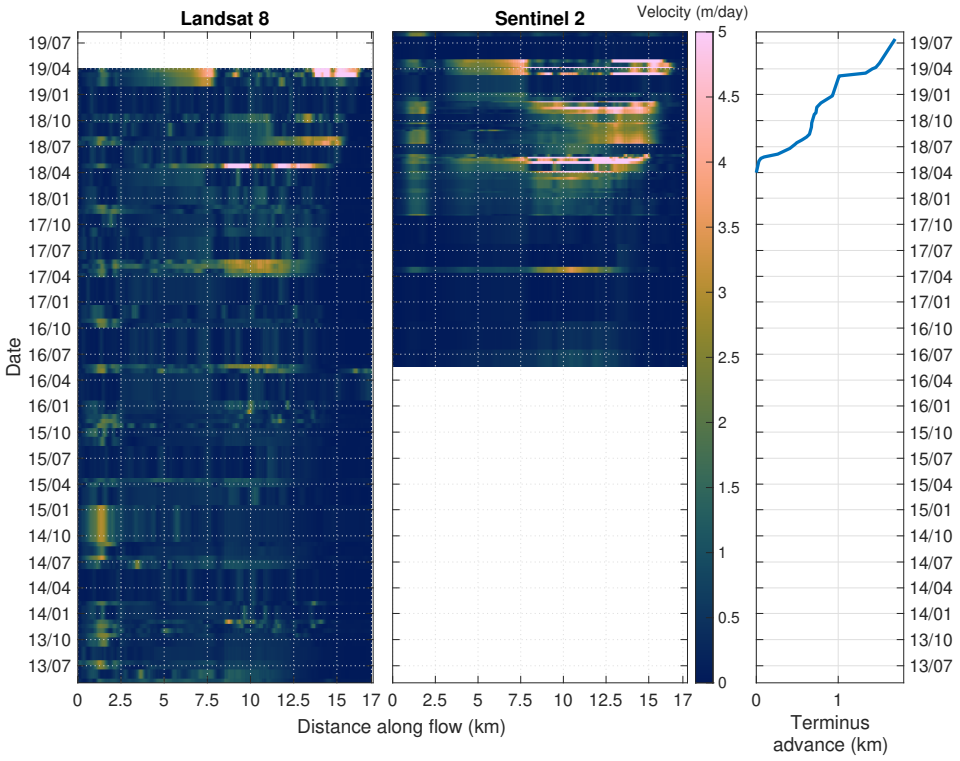

Figure S4.1. Comparison between velocity maps for Shisper glacier obtained with L8 and S2 data, with the terminus advance for reference. The data from L8 is useful to understand the surface velocities before the surge, in particular the presence of seasonal speed-ups and increase in amplitude of the spring speed-up leading up to the surge. The S2 data is limited temporally due to launch date, but it shines light on the surface velocity changes during the surge. The slow onset of the surge, the different phases and their link with terminus advances can only be made with S2 data.

S4.4 Axis scale rendering of sliding relationship

This section is similar to the previous one and focuses on axis scale. We show that whether we plot the data on a log-log or lin-lin scale, the qualitative conclusion in the manuscript hold.

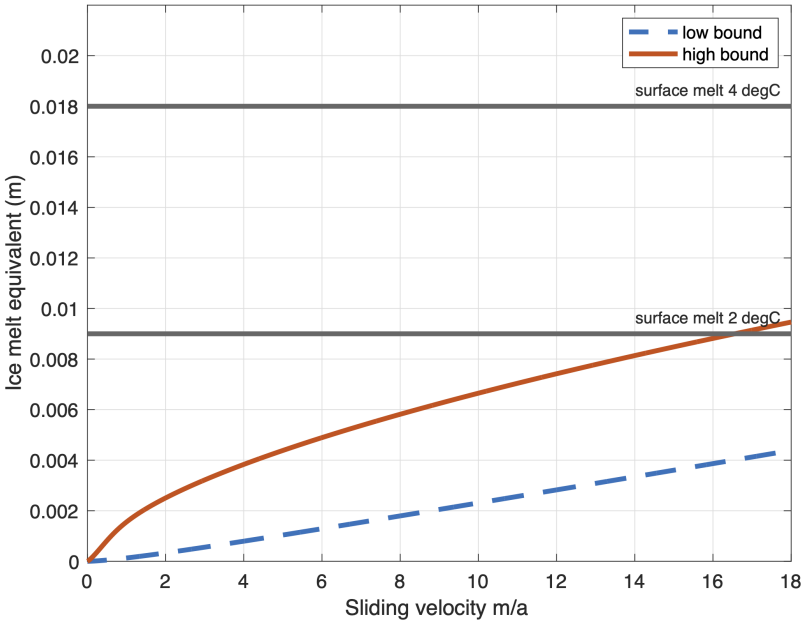

Figure S4.2. Estimation of ice melt in ice-thickness equivalent over $1\,\mathrm{m}^2$ calculated as a function of shear heating with the parameters in Table S4.1 compared with the expected surface melt for surface temperature of 2 and 4 degrees Celsius. These temperatures are what we observe in the re-analysis data around the times of Fall speed-ups for the main trunk zone. We used a degree day factor of 4.5, which is realistic for the Chinese Karakoram (Zhang et al., 2006)

References

Benn, D. I., Fowler, A., Hewitt, I. J., and Sevestre, H.: A general theory of glacier surges, Journal of Glaciology, 65, 701–716, 2019.

Farinotti, D., Huss, M., Fürst, J. J., Landmann, J., Machguth, H., Maussion, F., and Pandit, A.: A consensus estimate for the ice thickness distribution of all glaciers on Earth, Nature Geoscience, 12, 168, 2019.

Shah, A., Ali, K., Nizami, S., Jan, I., Hussain, I., and Begum, F.: Risk assessment of Shishper Glacier, Hassanabad Hunza, North Pakistan, Journal of Himalayan Earth Sciences Volume, 52, 1–11, 2019.

Zhang, Y., Liu, S., and Ding, Y.: Observed degree-day factors and their spatial variation on glaciers in western China, Annals of Glaciology, 43, 301–306, https://doi.org/10.3189/172756406781811952, 2006.

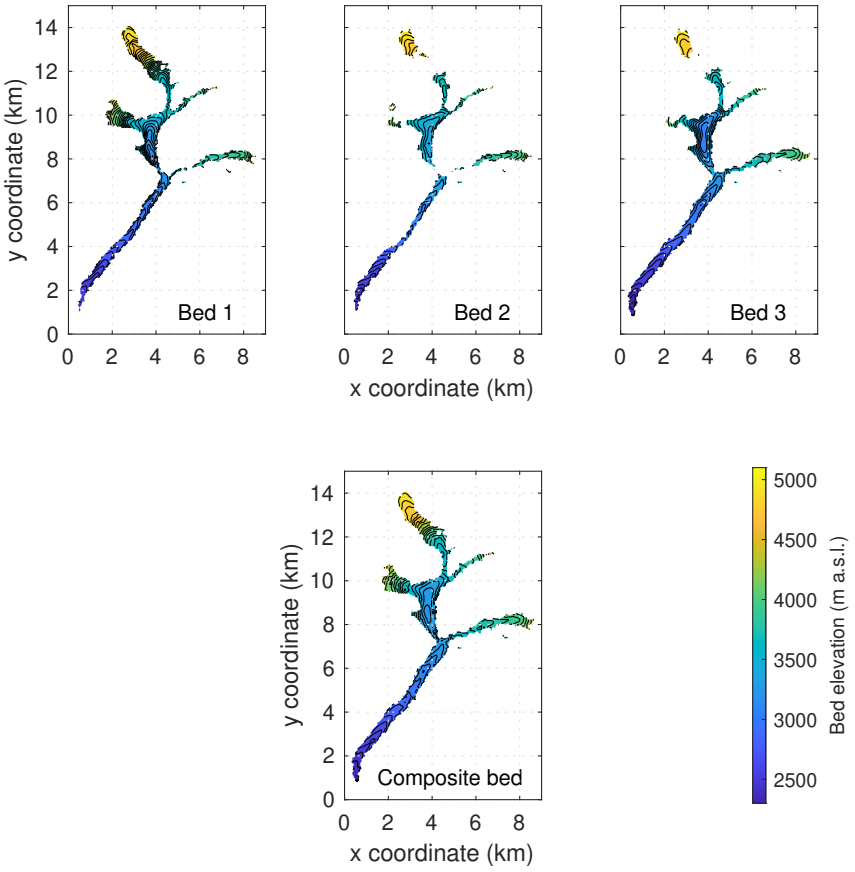

Figure S4.3. Different bed topography models for Shisper glacier from Farinotti et al. (2019).

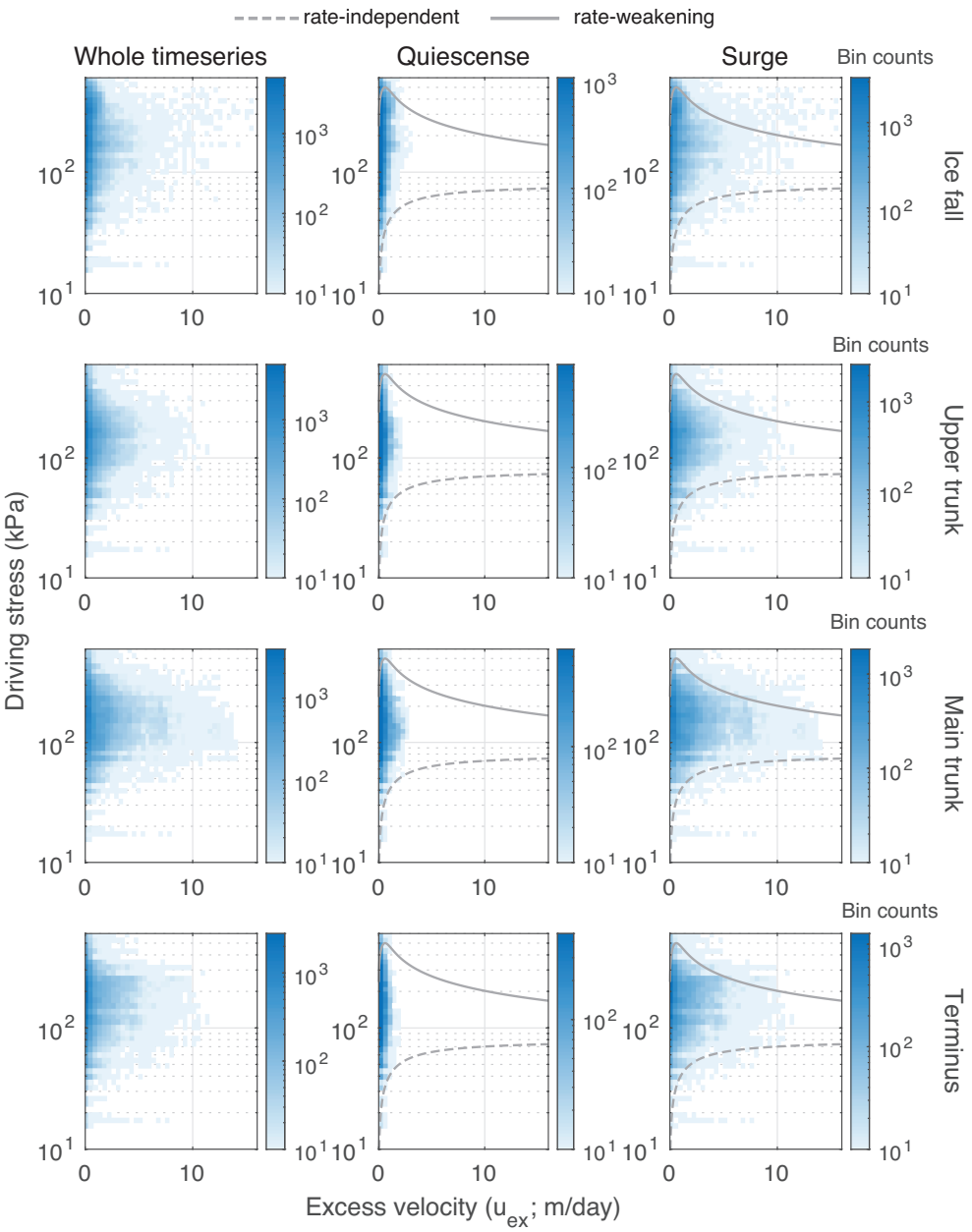

Figure S4.4. Driving stress calculated with SRTM DEM only plotted against excess velocity.

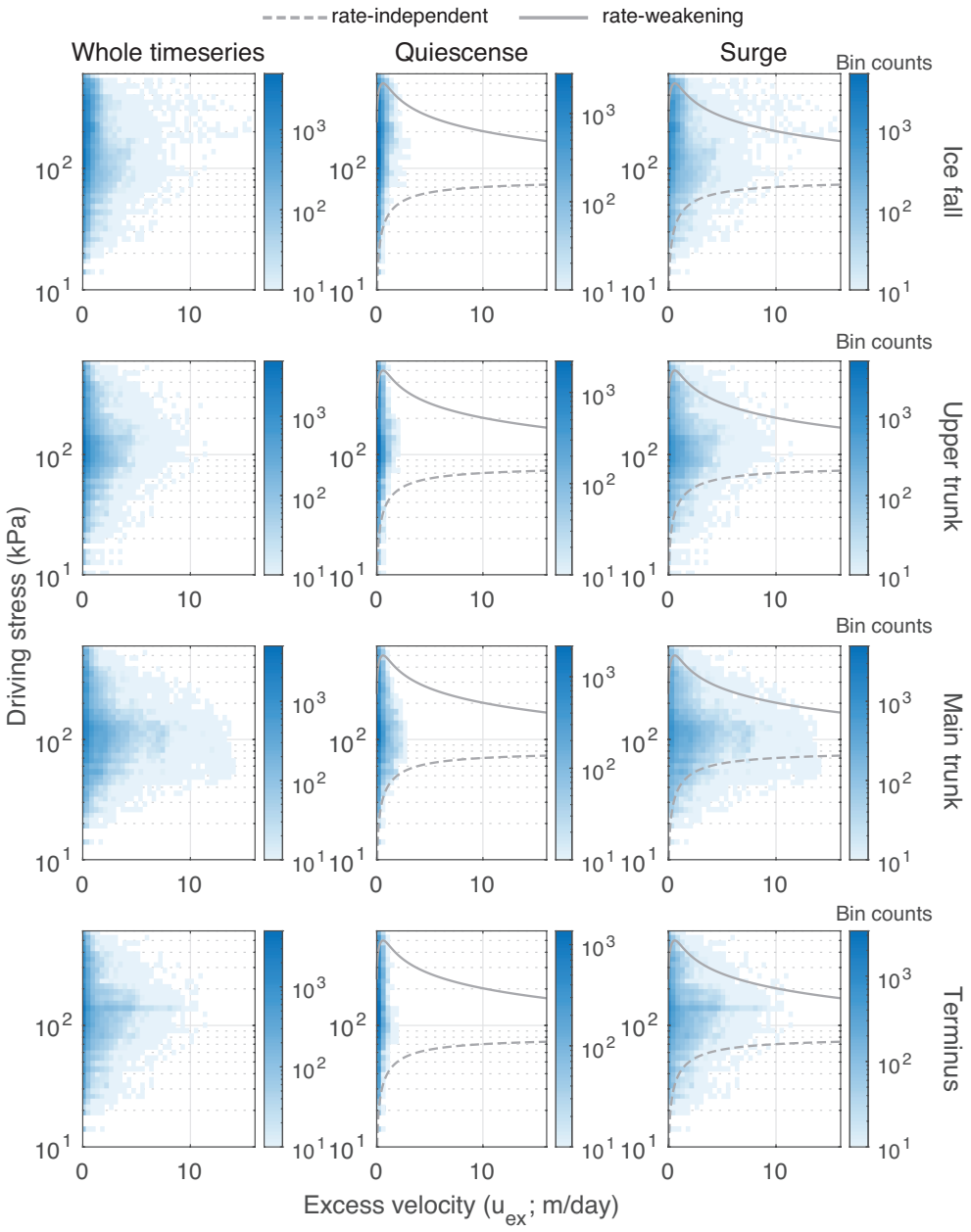

Figure S4.5. Driving stress calculated with 2019 Worldview DEM only plotted against excess velocity.

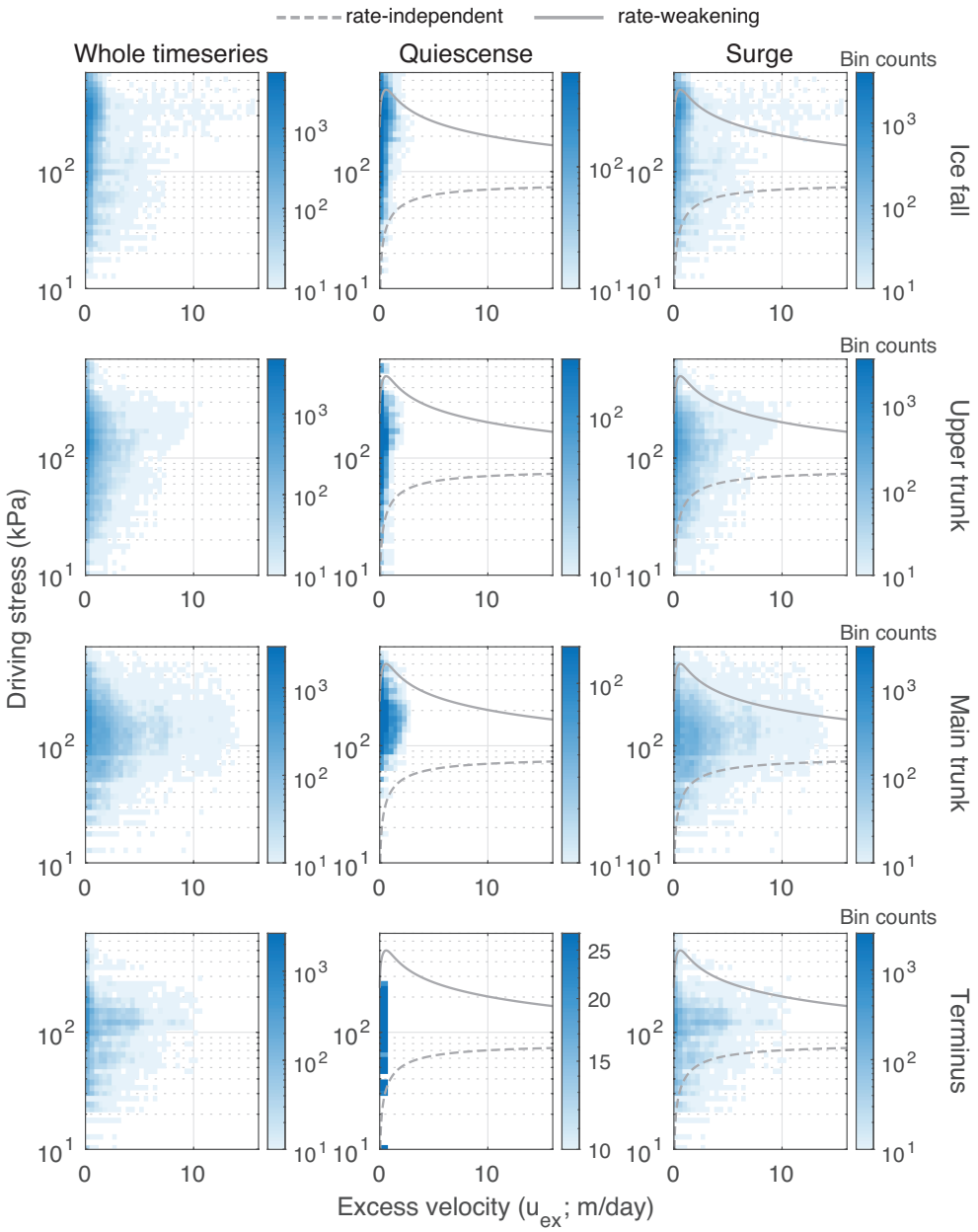

Figure S4.6. Driving stress calculated with the combination of SRTM and 2019 Worldview DEMs and the results from model 1 in Farinotti et al. (2019).

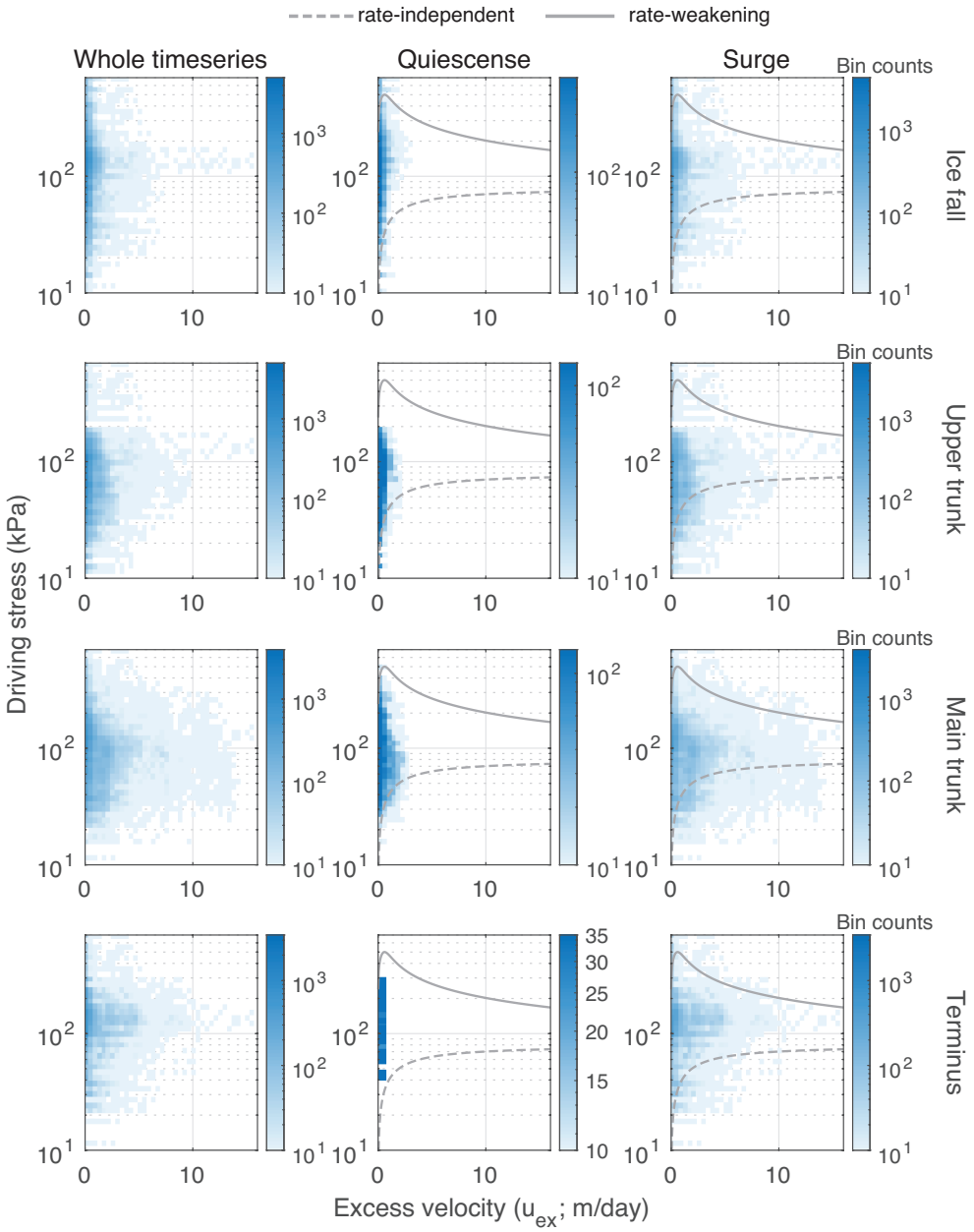

Figure S4.7. Driving stress calculated with the combination of SRTM and 2019 Worldview DEMs and the results from model 2 in Farinotti et al. (2019).

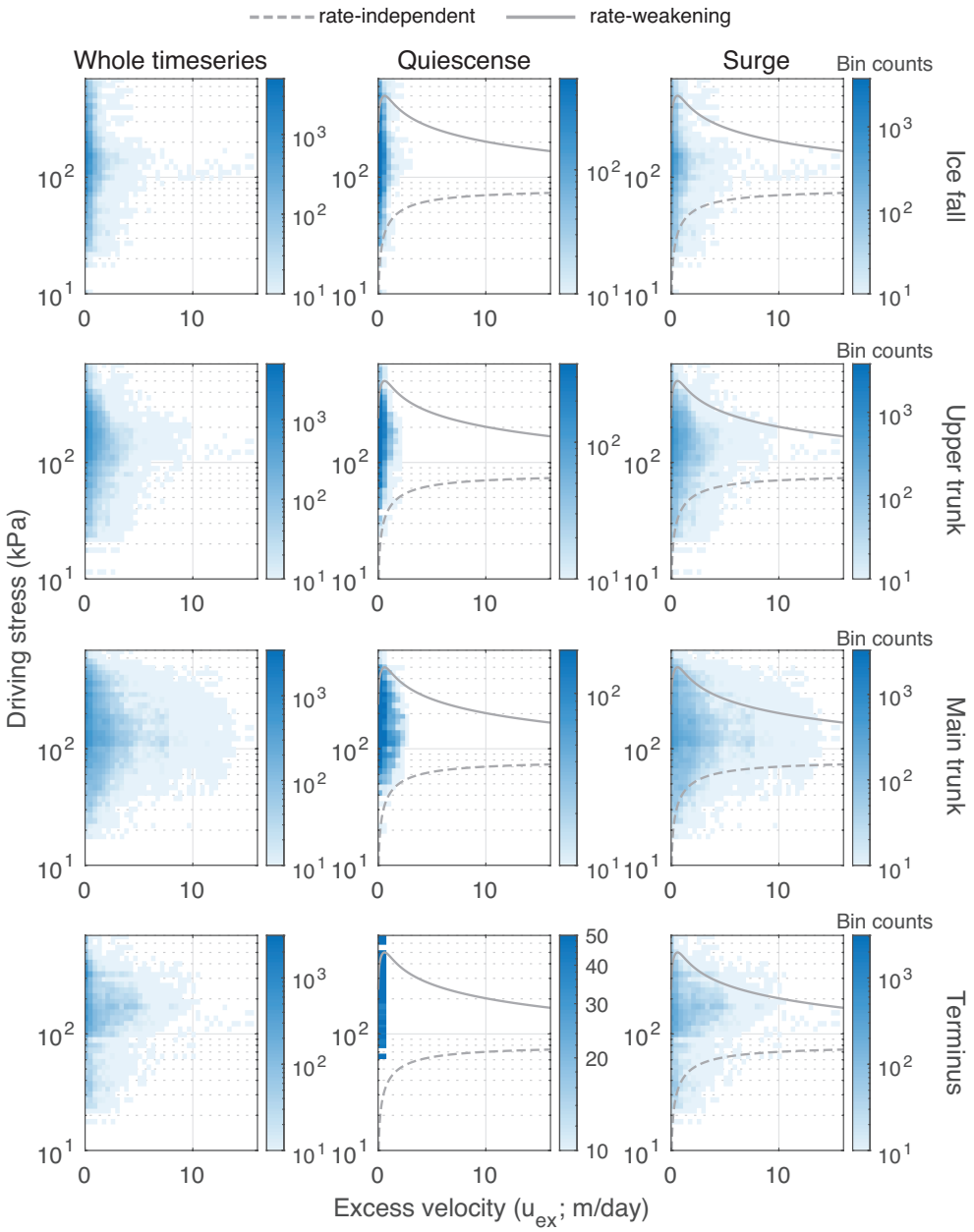

Figure S4.8. Driving stress calculated with the combination of SRTM and 2019 Worldview DEMs and the results from model 3 in Farinotti et al. (2019).

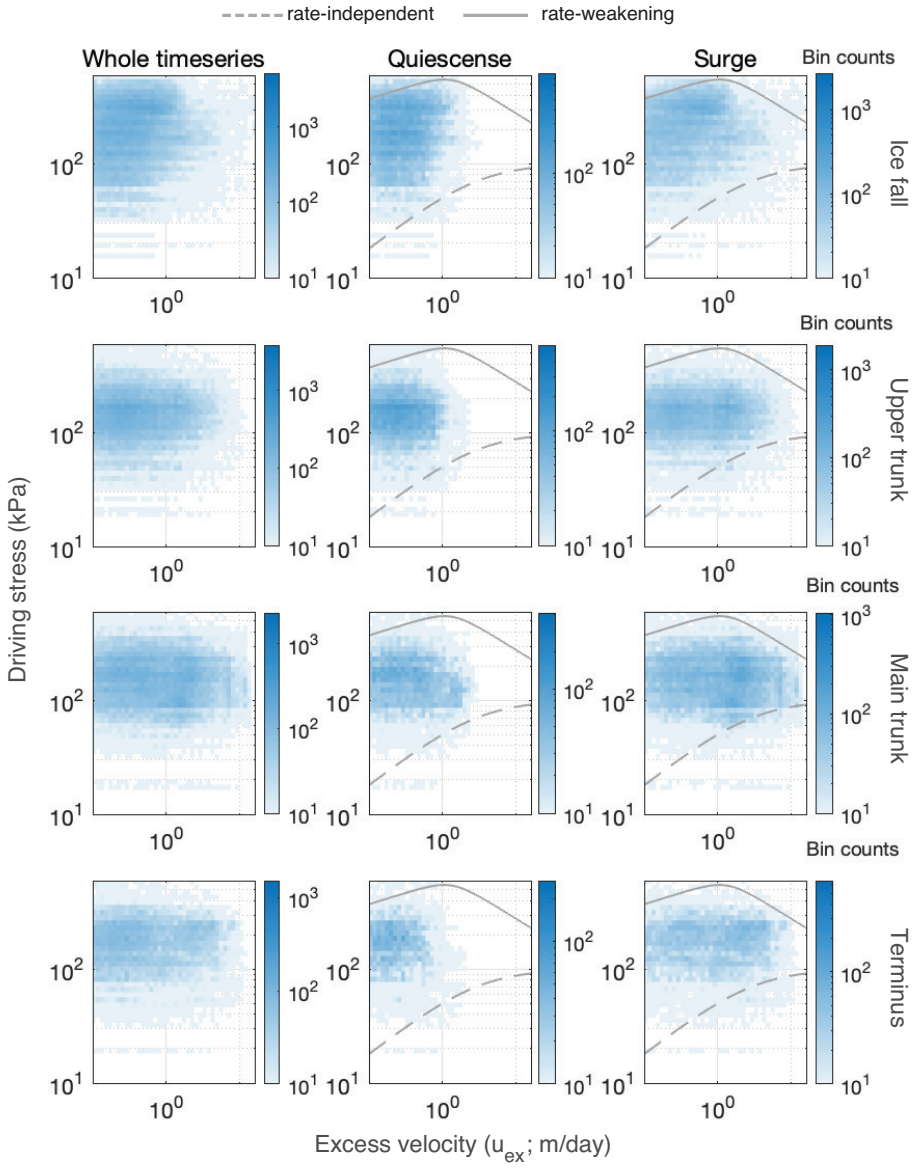

Figure S4.9. Relationship between driving stress and surface velocities departure from mean quiescence velocities with possible bounds by a unified glacier slip relationship (Eq. 6). Note that the Y and X-axes are logarithmic.

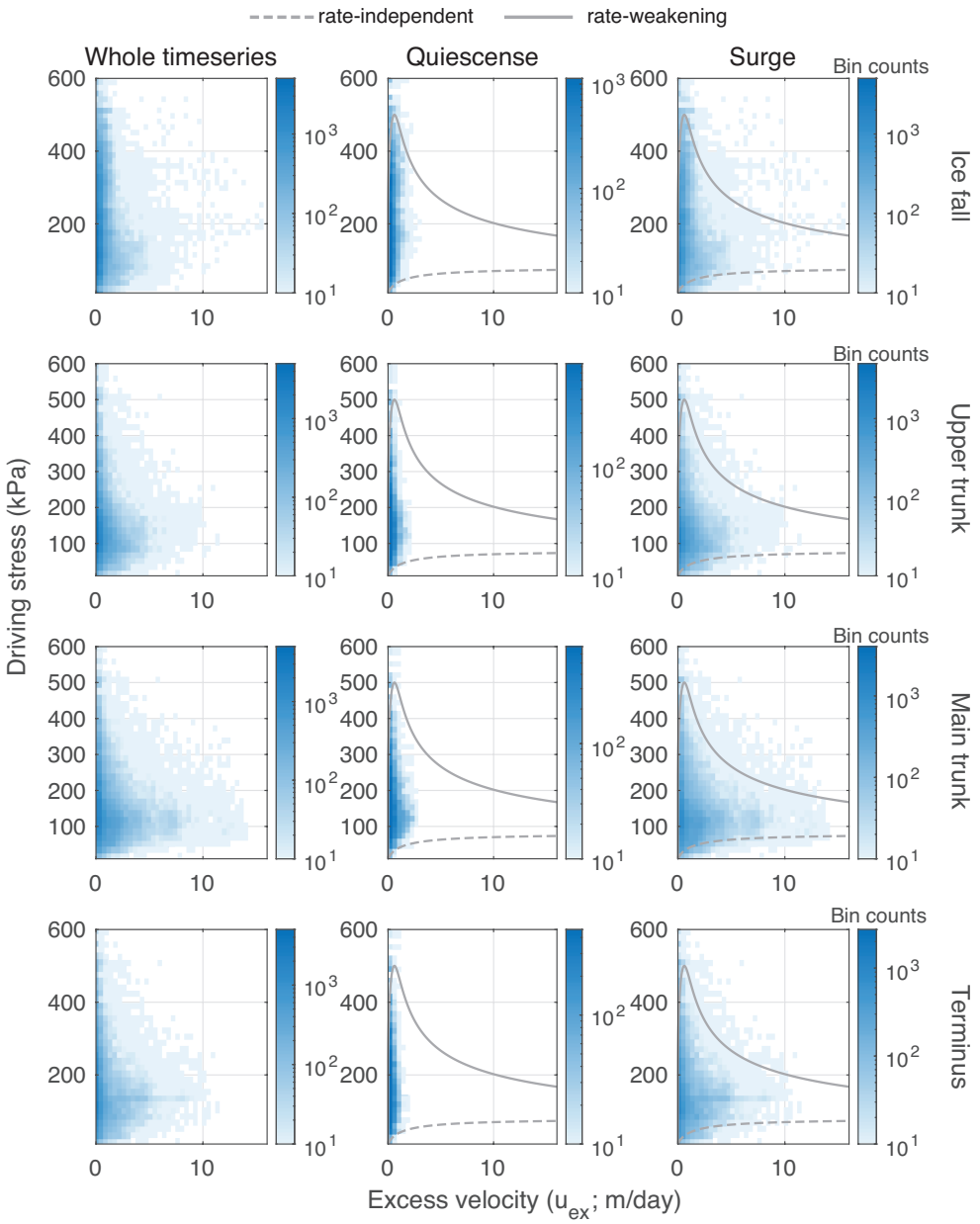

Figure S4.10. Relationship between driving stress and surface velocities departure from mean quiescence velocities with possible bounds by a unified glacier slip relationship (Eq. 6). Note that the Y and X-axes are linear.